

Notice: This manuscript has been authored by UTBatelle, LLC, under contract DE-AC05-00OR22725 with the US Department of Energy (DOE). The US government retains and the publisher, by accepting the article for publication, acknowledges that the US government retains a nonexclusive, paid-up, irrevocable, worldwide license to publish or reproduce the published form of this manuscript, or allow others to do so, for US government purposes. DOE will provide public access to these results of federally sponsored research in accordance with the DOE Public Access Plan (<http://energy.gov/downloads/doe-public-access-plan>).

# Observation of Large Magnetic Anisotropy and Field-induced Magnetic State in SrCo(VO<sub>4</sub>)(OH): A Structure with Quasi One-Dimensional Magnetic Chain

Liurukara D Sanjeewa,<sup>a,c\*</sup> V. Ovidiu Garlea,<sup>b</sup> Randy S. Fishman,<sup>a</sup> Michael McGuire,<sup>a</sup> Jie Xing,<sup>a</sup> Huibo Cao,<sup>b</sup> Joseph W. Kolis,<sup>c\*</sup> Athena S. Sefat<sup>a</sup>

<sup>a</sup>*Materials Science and Technology Division, Oak Ridge National Laboratory, Oak Ridge, Tennessee 37831, United States*

<sup>b</sup>*Neutron Scattering Division, Oak Ridge National Laboratory, Oak Ridge, Tennessee 37831, United States*

<sup>c</sup>*Department of Chemistry and Center for Optical Materials Science and Engineering Technologies (COMSET), Clemson University, Clemson, SC 29634-0973, USA*

*\*Corresponding Authors*

[sanjeewald@ornl.gov](mailto:sanjeewald@ornl.gov)

[kjoseph@clemson.edu](mailto:kjoseph@clemson.edu)

## Abstract

A new member of the Descolizite family, a cobalt vanadate, SrCo(VO<sub>4</sub>)(OH) has been synthesized as large single crystals using high-temperature and high-pressure hydrothermal methods. The SrCo(VO<sub>4</sub>)(OH) crystallizes in the orthorhombic crystal system in the space group of  $P2_12_12_1$  with unit cell parameters of  $a = 6.0157(2)$  Å,  $b = 7.645(2)$  Å,  $c = 9.291(3)$  Å,  $V = 427.29(2)$  Å<sup>3</sup>,  $Z = 4$ . It contains one-dimensional Co–O–Co chains of edge-sharing CoO<sub>6</sub> octahedra along the  $a$ -axis connected to each other via VO<sub>4</sub>-tetrahedra along the  $b$ -axis forming a three-dimensional structure. Magnetic susceptibility of SrCo(VO<sub>4</sub>)(OH) indicates an antiferromagnetic transition at 10 K as well as unusually large spin orbit coupling. Single crystal magnetic measurements in all three main crystallographic directions displayed a significant anisotropy in both temperature and field dependent data. Single crystal neutron diffraction at 4 K was used to characterize the magnetically ordered state. The Co<sup>2+</sup> magnetic spins are arranged in a staggered configuration along the chain direction, with a canting angle that follows the tipping of the CoO<sub>6</sub> octahedra. The net magnetization along the chain-direction resulting ferromagnetic coupling of the  $a$ -axis spin-components in each chain, is compensated by an antiferromagnetic interaction between nearest

neighbor chains. A metamagnetic transition appears in the isothermal magnetization data at 2 K along the chain direction, which seems to correspond to a co-alignment of the spin directions of the nearest neighbor chain. We propose a phenomenological spin-Hamiltonian that describes the canted spin configuration of the ground state and the metamagnetic transition in SrCo(VO<sub>4</sub>)(OH).

**Keywords:** *hydrothermal, crystal growth, vanadate, neutron diffraction, cobalt(II)*

## 1. Introduction

Magnetic materials with one dimensional (1D) chains built from edged sharing transition metal octahedra have attracted much attention due to their diverse exciting physical properties.<sup>1-3</sup> It is well known that there are examples of crystals with no long range magnetic ordering at the lowest observed temperatures in well isolated 1D magnetic materials made from spin ½ magnetic ions such as Cu<sup>2+</sup> or V<sup>4+</sup>.<sup>4-10</sup> A large number of 1D compounds display long range ordering due to interchain interactions through non-magnetic linking groups. Thus, most of the 1D compounds are categorized as pseudo-one-dimensional magnetic materials. The ordering temperatures of these pseudo one-dimensional compounds largely depend on the spin state of the magnetic ions and the competition between intra and inter-chain interactions in the structure. Additionally, the magnetic anisotropy could also lead to complex magnetic phase diagrams in this class of compounds, leading to interesting magnetic properties.<sup>11-14</sup>

Various mineral types with 1D magnetic chains are good candidates for such interesting magnetic phenomena.<sup>15</sup> The pyroxene class for example, has been studied in considerable detail. Pyroxene has a common formula of AMX<sub>2</sub>O<sub>6</sub> (A = Li, Na, M = Ti<sup>3+</sup>, V<sup>3+</sup>, Cr<sup>3+</sup>, Mn<sup>3+</sup> and Fe<sup>3+</sup>, X = Si<sup>4+</sup> or Ge<sup>4+</sup>). The general structure consists of 1D zigzag chains of edged sharing MO<sub>6</sub>, with the chains connected through XO<sub>4</sub> units to provide a quasi 1D magnetic structure. These compounds

display extremely rich magnetic properties depending on the *A*-site cation and the transition metal cation. For example, Ti-based pyroxenes exhibit spin-Peierls-like transitions while  $V^{3+}$ -based are known to be perfect Haldane-chain compounds with spin  $S = 1$  states.<sup>16-17</sup> A complete summary of pyroxene-type magnetic materials is given in Ref 11. Brackebuschite is another mineral type that has been synthesized containing  $V^{3+}$ ,  $Mn^{3+}$  and  $Fe^{3+}$  ions, and their bulk magnetic properties have been characterized.<sup>10</sup> These compounds possess completely isolated 1D chains made from edge sharing transition metal octahedra. Bulk magnetic measurements of  $Ba_2V(VO_4)_2(OH)$  ( $S=1$ ) reveals a broad maximum in magnetic susceptibility at  $\sim 100$  K with no sign of magnetic ordering down to 2 K suggesting spin-liquid behavior.<sup>10</sup> On the other hand, Brackebuschite-type  $Pb_2Mn(VO_4)_2(OH)$ , ( $S = 2$ ) exhibits a ferromagnetic transition at  $T_C = 14$  K.<sup>18</sup> Descloizite ( $Pb(Zn,Cu)(VO_4)(OH)$ ) is another mineral type where, in this case, divalent transition metal cations form the 1D chains compared to the more common trivalent transition metal cations chains in Pyroxene and Brackebuschite.<sup>19-20</sup> Recently, we have examined the bulk magnetic properties and magnetic structure of the Descloizite-type  $SrMn(VO_4)(OH)$  compound with  $S = 5/2$ .<sup>21</sup> The magnetic study reveals a broad maximum at approximately 80 K in magnetic susceptibility before antiferromagnetic order at  $T_N = 30$  K.<sup>21</sup> Single crystal neutron diffraction of  $SrMn(VO_4)(OH)$  revealed that Dzyaloshinskii-Moriya antisymmetric exchange interaction leads to slight spin canting that produces a weak ferromagnetism along the chain direction.

As discussed previously, mineral structures provide an excellent inspiration to investigate new materials with exciting magnetic properties.<sup>14</sup> Detailed magnetic measurement of naturally occurring minerals themselves is often complicated by the fact that the samples are usually contaminated with magnetic impurities such as iron, which mitigates their interesting magnetic properties. Therefore, a versatile synthetic method is essential to obtain clean samples and large

single crystals of mineral based compounds. Consequently, we use high-temperature high-pressure solution-based technique to access these mineralogically inspired magnetic materials and as well as other interesting related low-dimensional magnetic materials.<sup>15,23-26</sup> Recently we have been devoting our attention to transition metal vanadates. In contrast to phosphate ( $\text{PO}_4^{3-}$ ) and arsenates ( $\text{AsO}_4^{3-}$ ), vanadium can possess several oxidation states including  $\text{V}^{3+}$  ( $S = 1$ ),  $\text{V}^{4+}$  ( $S = 1/2$ ) in addition to the non-magnetic  $\text{V}^{5+}$ . Additionally, vanadium can form different oxy anions such as  $\text{VO}_4^{3-}$ ,  $\text{V}_2\text{O}_7^{4-}$  and  $\text{VO}_5^{2-}$ .<sup>27-29</sup> The vanadate ( $\text{V}^{5+}$ ) building blocks are non-magnetic but the presence of empty  $d$  orbitals in the bridging group could modify the Goodenough-Kanamori-Anderson super-exchange rules.<sup>30</sup>

This article focuses on Desclozite-type  $\text{SrCo}(\text{VO}_4)(\text{OH})$  with edge sharing chains of  $\text{Co-O-Co}$  made from  $\text{Co}^{2+}\text{O}_6$  octahedra, ( $S = 3/2$ ) and the  $\text{Co-O-Co}$  chains are interconnected with tetrahedral vanadate groups to provide a 3D structure. Large single crystals of  $\text{SrCo}(\text{VO}_4)(\text{OH})$  were synthesized using a high temperature hydrothermal method and anisotropic magnetic properties were determined by magnetic susceptibility measurements. The magnetic structure was determined by single crystal neutron diffraction. This compound exhibits a pronounced anisotropic behavior in its magnetic susceptibility, with a field induced metamagnetic transition along the  $\text{Co-O-Co}$  chain direction (the  $a$ -axis). Interestingly, neutron diffraction confirms that the magnetic spins are arranged ferromagnetically along the chain direction, but are antiferromagnetic between the chains.

## 2. Experimental Section

### 2.1. Hydrothermal Synthesis of $\text{SrCo}(\text{VO}_4)(\text{OH})$

Hydrothermal crystal growth of SrCo(VO<sub>4</sub>)(OH) was performed using 2.75-inch long silver tubing that had an inner diameter of 0.375 inches. After silver tubes were welded shut on one side the reactants and the mineralizer were added. The silver ampoules were then welded shut and placed in a Tuttle-seal autoclave filled with water in order to provide appropriate counter pressure. The autoclaves were then heated to 580 °C for 10 days, reaching an average pressure of 1.7 kbar. Crystals were recovered by washing with de-ionized water. Synthesis of SrCo(VO<sub>4</sub>)(OH) single crystals were achieved using a mixture of SrO, Co<sub>3</sub>O<sub>4</sub> and V<sub>2</sub>O<sub>5</sub> with CsOH mineralizer. A typical reaction consist with 0.4 g of total reactants (SrO: 0.0788g; Co<sub>3</sub>O<sub>4</sub>: 0.1830 g; V<sub>2</sub>O<sub>5</sub>: 0.1382 g) in the stoichiometric ratio of 1 : 1 : 1 with 0.8 mL of 5 M CsOH. The single crystal specimen of SrCo(VO<sub>4</sub>)(OH) in Figure 1a (4 mg) was used in both magnetic property characterizations and single crystal neutron diffraction. The chemical reagents were used as they received from the supplier: SrO (Alfa Aesar, 99.9%), Co<sub>3</sub>O<sub>4</sub> (Alfa Aesar, 99.9%), and V<sub>2</sub>O<sub>5</sub> (Alfa Aesar, 99.6%).

## 2.2. X-Ray Diffraction

Crystals of SrCo(VO<sub>4</sub>)(OH) were physically examined and selected under an optical microscope equipped with a polarizing attachment. The crystals of SrCo(VO<sub>4</sub>)(OH) were mounted on a glass fiber with epoxy. Room temperature single crystal X-ray diffraction data were collected using a four-circle Rigaku AFC8 diffractometer equipped with a Mercury CCD area detector, MoK $\alpha$  ( $\lambda = 0.71073 \text{ \AA}$ ) radiation. Data collection, processing, and scaling were performed using CrystalClear software suites.<sup>31</sup> The structures were solved by direct methods and refined by full-matrix least-squares on  $F^2$  using the SHELXTL software suite.<sup>32</sup> All non-hydrogen atoms were refined anisotropically. In the cases of OH<sup>-</sup> group, hydrogen atom positions were identified from the difference electron density map, and their occupancies were set to confirm to realistic geometries

in accord with electroneutrality requirements. Table 1 provides the details unit cell parameters with selected bond distances in Table 2. Further, crystallographic orientations were also determined using the single crystal X-ray diffractometer.

### *2.2 Magnetic property characterization*

Temperature-dependent and field dependent magnetic measurements were performed using a Quantum Design Magnetic Property Measurement System (MPMS). Here, the single crystal specimen was affixed to a quartz rod using GE varnish and the magnetic properties perpendicular to the flat surface of the single crystal was performed by sandwiching the single crystal between two quartz rods. The temperature dependent magnetization measurements were carried out along all three crystallographic directions from 2 to 300 K in the applied magnetic field of 10 kOe and 40 kOe. Similarly, isothermal magnetization measurements were performed at 2, 50 and 300 K up to 50 kOe magnetic field. Heat-capacity measurements of  $\text{SrCo}(\text{VO}_4)(\text{OH})$  were performed using Physical Property Measurement System (PPMS, Quantum Design) in zero and 40 kOe applied magnetic field.

### *2.3 Neutron scattering*

Single crystal neutron diffraction data were collected using the HB3A four-circle diffractometer at the High Flux Isotope Reactor at Oak Ridge National Laboratory.<sup>33</sup> For the data collection  $\text{SrCo}(\text{VO}_4)(\text{OH})$  single crystal was glued to an aluminum pin and loaded into a closed-cycle-refrigerator which provides sample temperature control within the window of 4-300 K. A wavelength of 1.542 Å was selected by a Si-220 monochromator.

**Table 1.** Crystallographic data of SrCo(VO<sub>4</sub>)(OH) determined by single crystal X-ray diffraction.

empirical formula	SrCo(VO <sub>4</sub> )(OH)
formula weight (g/mol)	278.50
crystal system	orthorhombic
Crystal dimensions, mm	0.16 x 0.10 x 0.08
space group, <i>Z</i>	<i>P</i> 2 <sub>1</sub> 2 <sub>1</sub> 2 <sub>1</sub> (no.19), 4
<i>T</i> , K	298
<i>a</i> , Å	6.0157(2)
<i>b</i> , Å	7.645(2)
<i>c</i> , Å	9.291(3)
volume, Å <sup>3</sup>	427.30(2)
<i>D</i> (calc), g/cm <sup>3</sup>	4.329
$\mu$ (Mo K $\alpha$ ), mm <sup>-1</sup>	18.323
<i>F</i> (000)	516
<i>T</i> <sub>max</sub> , <i>T</i> <sub>min</sub>	1.0000, 0.5158
2 $\theta$ range	3.382-26.050
reflections collected	3953
data/restraints/parameters	844/1/79
final <i>R</i> [ <i>I</i> > 2 $\sigma$ ( <i>I</i> )] <i>R</i> <sub>1</sub> , <i>R</i> <sub>w2</sub>	0.0253, 0.0586
final <i>R</i> (all data) <i>R</i> <sub>1</sub> , <i>R</i> <sub>w2</sub>	0.0239, 0.0578
GoF	1.107
largest diff. peak/hole, e/Å <sup>3</sup>	0.0696/-0.832
Flack parameter	0.38(2)

**Table 2.** Selected bond distances (Å) and angles (°) of SrCo(VO<sub>4</sub>)(OH).

<b>Co(1)O<sub>6</sub></b>	
Co(1)–O(1)	1.976(5)
Co(1)–O(1)	1.981(6)
Co(1)–O(2)	2.147(5)
Co(1)–O(2)	2.222(5)
Co(1)–O(3)	2.183(6)
Co(1)–O(4)	2.198(5)
<b>V(1)O<sub>4</sub></b>	
V(1)–O(2)	1.734(5)
V(1)–O(3)	1.730(5)
V(1)–O(4)	1.718(5)
V(1)–O(5)	1.687(5)
Co(1)–O(1)–Co(1)	99.08(3)
Co(1)–O(2)–Co(1)	87.13(3)
Co···Co	3.011(3)

### 3. Results and Discussion

#### 3.1. Crystal structure of $\text{SrCo}(\text{VO}_4)(\text{OH})$

$\text{SrCo}(\text{VO}_4)(\text{OH})$  crystallizes in orthorhombic crystal system in the space group of  $P2_12_12_1$  (no.19). The room temperature unit cell parameters are  $a = 6.0157(15)$  Å,  $b = 7.645(2)$  Å,  $c = 9.291(3)$  Å and  $V = 427.30(2)$  Å<sup>3</sup>. Significant crystallographic parameters, bond distances and angles are summarized in Table 1 and 2, respectively. The detailed crystallographic data including *Wyckoff* positions and thermal parameters are given under Supporting Information, Table S1. The material is isostructural with  $\text{SrMn}(\text{VO}_4)(\text{OH})$ -dezscolazite. A detailed structural discussion of  $\text{SrCo}(\text{VO}_4)(\text{OH})$  given below, is important for the understanding of the magnetic structure compared to  $\text{SrMn}(\text{VO}_4)(\text{OH})$ . The structure is comprised of individual crystallographically independent  $\text{Sr}^{2+}$ ,  $\text{Co}^{2+}$  and  $\text{V}^{5+}$  sites. The  $\text{Co}^{2+}$  form distorted octahedra forming edge shared one-dimensional (1D) Co–O–Co chains along the *a*-axis (Figure 1b and c). The  $\text{VO}_4$  tetrahedra connect the 1D Co–O–Co chains to each other along the *bc*-plan imparting a three dimensional nature to  $\text{SrCo}(\text{VO}_4)(\text{OH})$ . The Co–O bond lengths vary from 1.976(5) to 2.222(5) Å highlighting the distortion in the  $\text{CoO}_6$  octahedra, while the O–Co–O bond angles vary from 85.8(2)° and 97.1(4)°. The  $\text{CoO}_6$  units interconnected via O(1) and O(2) sharing edges. It is noteworthy that, Co–O(1) and Co–O(2) form the shortest and longest Co–O bonds within the  $\text{CoO}_6$  octahedra, respectively, Figure 1c. The edged sharing O(1) are also bound to H generating the OH group in the structure. The other oxygen atoms (O(2), O(3) and O(4)) connect with  $\text{VO}_4$  tetrahedral groups in an up and down fashion along the cobalt oxide chains, Figure 1c. Each  $\text{VO}_4$  tetrahedral group shares edges with one Co–O–Co chain via O(3) and O(4) and is corner shared with another Co–O–Co chain via O(2) along the *bc*-plan, Figure 1c. The V–O bond lengths in the  $\text{VO}_4$  tetrahedra range from 1.687(5) to 1.718(5) Å.

Since  $V^{5+}$  is non-magnetic, the  $VO_4$  groups generate structurally confined 1D  $Co-O-Co$  chains along the  $a$ -axis. However, interchain interactions are possible via the  $Co-O-V-O-Co$  connectivity. Figure 2 highlights the distance between  $Co^{2+}$  sites within the chain, which is  $3.011(3) \text{ \AA}$ , while the shortest interchain cobalt-cobalt distance is  $5.951(5) \text{ \AA}$ . Further, the  $Co-O(1)-Co$  and  $Co-O(2)-Co$  bond angles are  $87.13(3)^\circ$  and  $99.08(3)^\circ$ . Compared to  $SrMn(VO_4)(OH)$ , the  $M-O-M$  angles are slightly larger in  $SrCo(VO_4)(OH)$  ( $Mn-O-Mn$  bond angles are  $86.68(8)^\circ$  and  $96.69(9)^\circ$ ), while the intrachain metal-metal distance is very similar. Additionally, the shortest interchain  $Mn-Mn$  distance in  $SrMn(VO_4)(OH)$  is  $6.004(3) \text{ \AA}$ . These subtle structural changes and the different spin state lead to different magnetic properties for  $SrCo(VO_4)(OH)$  compared to the manganese analog.

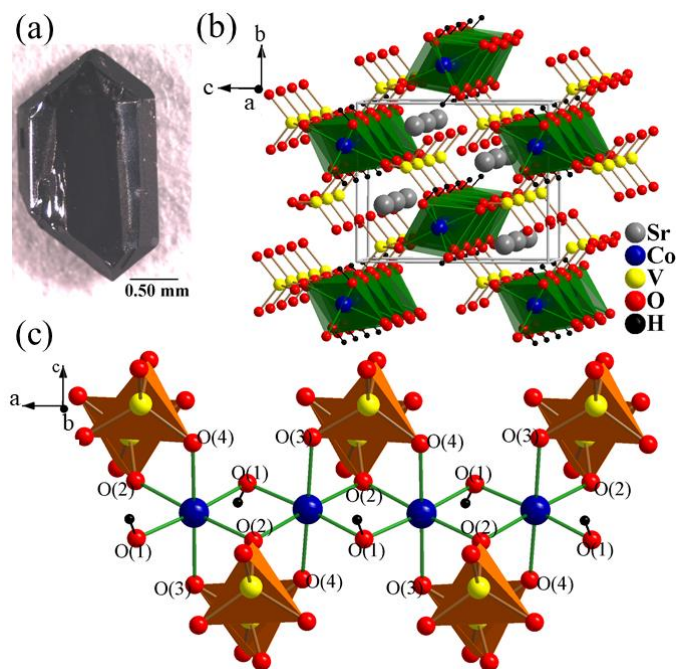


**Figure 1.** (a) Hydrothermally grown single crystal of  $SrCo(VO_4)(OH)$ . (b) The view of  $SrCo(VO_4)(OH)$  projected along the  $a$ -axis, showing packing of  $Co-O-Co$  chains along the  $bc$ -plane. The  $Sr^{2+}$  ions reside between the channels made from  $CoO_6$  octahedra (green polyhedra) and  $VO_4$  tetrahedra. (c) Partial structure of  $Co-O-Co$  chains made from edged sharing  $CoO_6$  octahedra along the  $a$ -axis. The  $VO_4$  tetrahedra (orange polyhedra) connect with  $Co-O-Co$  chains in an up and down fashion along the chain. Hydrogen atoms connect to O(1) forming the only OH group in the structure.

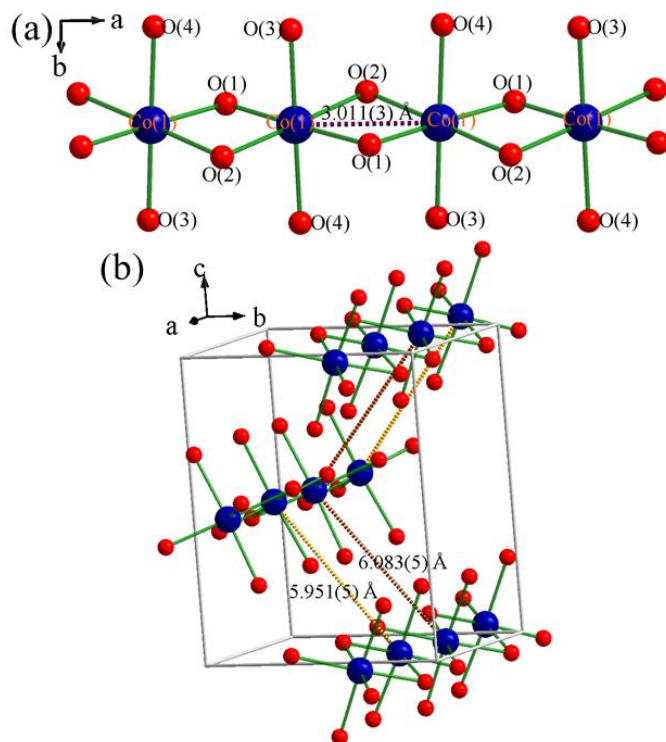


**Figure 2.** (a) A fragment of the Co–O–Co chain along the *a*-axis showing the edged sharing connectivity of the CoO<sub>6</sub> octahedra. The intrachain distance between two Co is highlighted by purple dotted line, 3.011(3) Å. (b) The interchain distances are highlighted in orange dotted lines. The shortest distance between the chains is 5.951(5) Å.

### 3.2 Magnetic Properties of SrCo(VO<sub>4</sub>)(OH)

Magnetic properties of SrCo(VO<sub>4</sub>)(OH) were examined by magnetic susceptibility (field cooling mode), isothermal magnetization and heat capacity. Both magnetic susceptibility and the isothermal magnetization were performed in three crystallographic directions. Figure 3 shows the magnetic susceptibility measured at 10 kOe applied magnetic field along the *a*, *b*, and *c*, directions. The magnetic susceptibility along the *a*-axis, which is the Co–O–Co chain direction, sharply rises with lowering the temperature reaching to a maximum value at 10 K and then decreases rapidly, suggesting antiferromagnetic ordering at  $T_N = 10$  K. Compared to the *a*-direction, the susceptibility along other two crystallographic directions do not exhibit a sharp increase with lowering temperatures indicating a strong anisotropy, with the magnetic easy axis oriented along the chain

direction. A significant anisotropic behavior of the susceptibility curves was observed even in the paramagnetic regime. Similar behavior has been observed in  $\text{BaCo}_2\text{V}_2\text{O}_8$  and  $\text{CoV}_2\text{O}_6$ , contain 1D  $\text{Co}^{2+}$  edge shared octahedra chains like the compound in this study. This behavior could be attributed to the large single-ion anisotropy due to spin orbital coupling of  $\text{Co}^{2+}$  and to the quasi-one dimensionality nature of the magnetic interactions.<sup>33-34</sup> Figure 3 inset shows the magnetization as a function of applied magnetic fields of 10 kOe and 40 kOe in all three crystallographic directions. Here, 10 kOe and 40 kOe temperature dependent magnetic susceptibility data along the  $b$ - and  $c$ -directions almost overlap with each other indicating no field dependent. However, when the applied magnetic field is oriented along the  $a$ -direction, in the higher field magnetic susceptibility continuously increases without showing a peak at 10 K. This indicates a field induced magnetic transition along the chain direction. The magnetic susceptibility measured in 10 kOe field was used for Curie-Weiss fits. The Curie-Weiss fits were performed for all three crystallographic directions using the data between 200 and 300 K. The fits produced  $\Theta_{\text{CW}}$  of 8 K, -47 K and -181 K along  $a$ -,  $b$ -,  $c$ -axis, respectively. Additionally, effective magnetic moments in three different directions are  $5.4 \mu_{\text{B}}$ ,  $5.2 \mu_{\text{B}}$  and  $4.9 \mu_{\text{B}}$ , respectively. These values are higher than the spin only value of  $\text{Co}^{2+}$  with  $S = 3/2$ ,  $\mu_{\text{eff}} = 3.8 \mu_{\text{B}}$ . This could be due to the significant orbital contribution since orbital moments are unquenched for  $\text{Co}^{2+}$  in octahedral environment ( $t_{2g}^5 e_g^2$ ,  $S = 3/2$ ,  $L = 3$ ). Similar higher values have been observed previously for 1D  $\text{Co}^{2+}$  chains compounds such as  $\text{CoV}_2\text{O}_6$  (saturated moment:  $4.4 \mu_{\text{B}}$ ) ( $\text{BaCo}_2\text{V}_2\text{O}_8$  ( $5.20 \mu_{\text{B}}$ ),  $\text{CoSe}_2\text{O}_5$  ( $5.20 \mu_{\text{B}}$ ),  $\text{Na}_4\text{CoTeO}_6$  ( $5.14 \mu_{\text{B}}$ ) and  $\text{NaCoSO}_4\text{F}$  ( $5.20 \mu_{\text{B}}$ ).<sup>33-39</sup> Further, effective magnetic moments in all three crystallographic directions do not deviate largely from each other. In contrast, a large deviation was observed in the Curie-Weiss temperatures. Therefore, we fitted the average magnetic susceptibility data obtained by averaging the magnetic susceptibilities along all three

crystallographic directions. The fitted  $\Theta_{CW}$  and effective magnetic moments are -36 K and  $5.05 \mu_B$ , respectively which further confirms the dominant antiferromagnetic interactions of  $\text{SrCo}(\text{VO}_4)(\text{OH})$ .<sup>34,35,38</sup>

Figure 4 displays the isothermal magnetization of  $\text{SrCo}(\text{VO}_4)(\text{OH})$  measured along three different crystallographic directions. The data were collected at 2-50 K. Below the  $T_N$ , a significant field dependence was observed in all three directions. An extremely sharp upturn (metamagnetic transition) was observed along the  $a$ -directions which is the Co–O–Co chain direction. This metamagnetic transition along the  $a$ -direction occurs at approximately 27 kOe and it could be due to the spin rearrangement from antiferromagnetic ground state to a ferromagnetic state. This behavior agrees well with our magnetic susceptibility data observed along the  $a$ -axis. Additionally, the change of magnetization ( $\Delta M (H=0)$ ) at the field induced transition is  $\sim 2 \mu_B/\text{Co}$  which further agrees with our refined magnetic moment projections obtained from our neutron diffraction data (see discussion below). Above the metamagnetic transition, the magnetization continuously rises approaching a  $2.7 \mu_B$  per Co at 70 kOe. At the same time, isothermal magnetizations measured at other two directions below 10 K ( $T_N$ ) do not show steep transition, however there is a slight curvature associated in each. This suggests that, Co spins rotate towards the  $a$ -axis by producing ferromagnetic state. It is worth noting that, the overall magnetism observed in  $\text{SrCo}(\text{VO}_4)(\text{OH})$  is very similar to  $\text{CoV}_2\text{O}_6$  where both compounds have 1D Co–O–Co chain made from highly distorted  $\text{Co}^{2+}\text{O}_6$  octahedra.<sup>33</sup> In  $\text{CoV}_2\text{O}_6$ , a large difference of magnetic susceptibility was observed in different crystallographic directions ( $c$ -axis is the magnetic easy axis) even at room temperature. Further, isothermal magnetization measured at 5 K exhibits a staircase magnetization curve along the Co–O–Co chain direction ( $c$ -axis) and a linear behavior in other two directions ( $a$ - and  $b$ -axis). A first jump in isothermal magnetization along the  $c$ -axis was observed at 16 kOe

reaching to  $1.4 \mu_B/\text{Co}$ , followed by a second jump at 33 kOe and a saturation of magnetization to  $4.4 \mu_B/\text{Co}$  at about 40 kOe. The saturated magnetic moment is much larger than the spin only value of  $\text{Co}^{2+}$  ( $3 \mu_B/\text{Co}$ ) which was described as an indication of large orbital contribution from distorted  $\text{CoO}_6$  oxygen environment.<sup>33</sup>

Heat capacity ( $C_p$ ) measurements of  $\text{SrCo}(\text{VO}_4)(\text{OH})$  were performed between 30 and 2 K at zero applied magnetic field and the 40 kOe applied magnetic field. The results are shown in Figure 5. Here field was applied along the  $c$ -axis of the single crystal. Zero field heat capacity displays a sharp peak at 10 K that corresponds to the  $T_N$  observed in magnetic susceptibility. There is a little effect from applying 40 kOe field along the  $c$ -axis with 0.3 K shift to the lower temperature which is consistent with magnetization data and this could be due to a small reorientation of the spin axis.<sup>36</sup> To calculate the magnetic entropy, the heat capacity data of  $\text{SrCo}(\text{VO}_4)(\text{OH})$  above 15 K were fitted by  $C_p = \gamma T + \beta_1 T^3 + \beta_2 T^5 + \beta_3 T^7$  where  $\gamma = 0$  for an insulator and  $\beta_1 T^3 + \beta_2 T^5 + \beta_3 T^7$  is the contribution from the lattice ( $C_l$ ). Therefore, magnetic contribution,  $C_m$ , was calculated as the difference of  $C_p - C_l$ . The magnetic entropy,  $S_M$ , was estimated by integrating  $C_{\text{mag}}/TdT$ . As displaying in Figure 5 inset, the magnetic entropy calculated is  $S_M = 4.43 \text{ J mol}^{-1} \text{ K}^{-1}$ . The expected entropy ( $\Delta S$ ) for  $\text{Co}^{2+}$  in  $S = 3/2$  spin state is  $11.5 \text{ J mol}^{-1} \text{ K}^{-1}$  ( $\Delta S = R \ln(2S+1)$ ) and observed magnetic entropy is 38% from  $R \ln(2S+1)$ . This difference could be attributed to the highly anisotropic behavior as we observed in magnetic susceptibility. Further, a relatively smaller magnetic entropy has been observed in 1D compounds such as  $\text{CoSe}_2\text{O}_5$ ,  $\text{Pb}_2\text{Co}(\text{V}_2\text{O}_7)(\text{OH})\text{Cl}$  and  $\text{SrMn}(\text{VO}_4)(\text{OH})$ .<sup>20,36,40</sup>

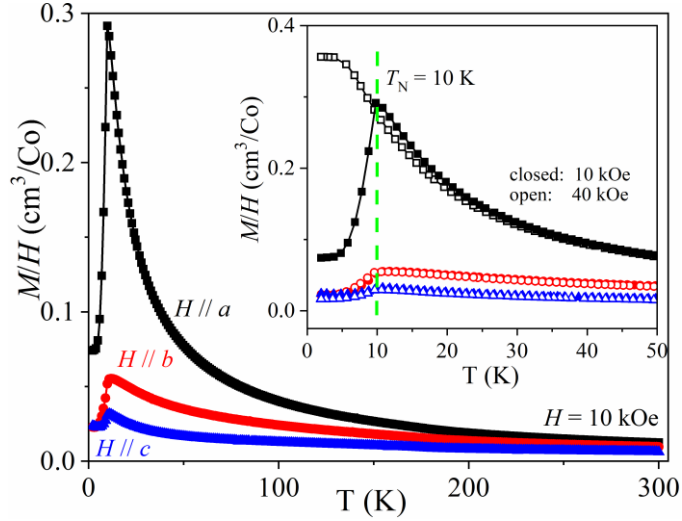


**Figure 3.** Susceptibility data of SrCo(VO<sub>4</sub>)(OH) measured at 10 kOe in three different crystallographic axes. Inset: Comparison of susceptibility data at 10 kOe and 40 kOe (open symbol) in all three crystallographic directions. Susceptibility along the chain axis shows a significant difference with the applied magnetic field (All the data collected in field cooling mode).

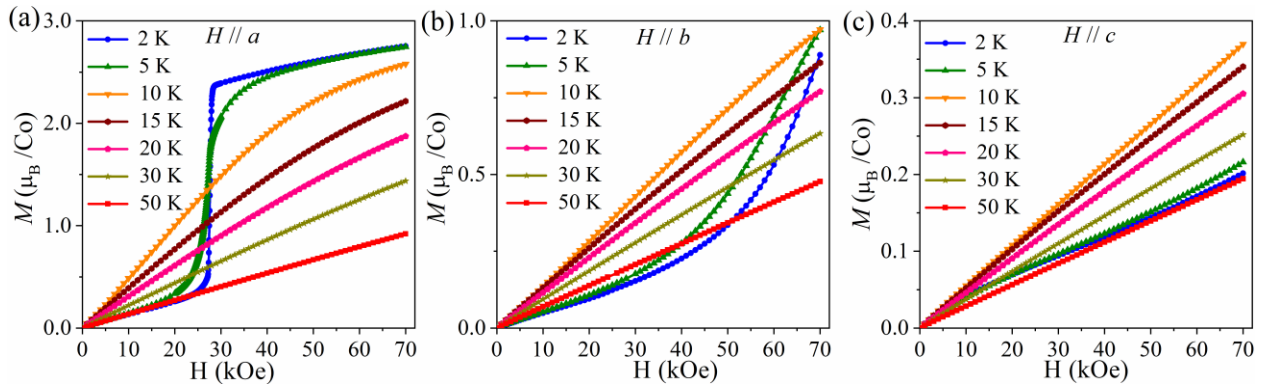


**Figure 4.** Field dependent data obtained by applying the magnetic field along the *a*-, *b*-, and *c*-directions. A sharp metamagnetic transitions was observed along *a*-axis at 27 kOe with slight curvature observed along the other two directions at 2 K.

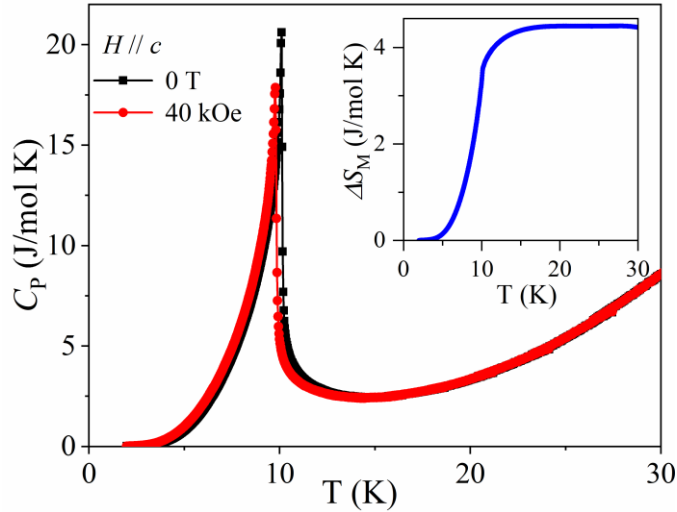


**Figure 5.** Heat capacity measured at  $H = 0$  and  $H = 40$  kOe exhibiting a sharp anomaly at the magnetic ordering temperature. The inset shows the magnetic entropy of  $\text{SrCo}(\text{VO}_4)(\text{OH})$ .

### 3.3 Magnetic Structure of $\text{SrCo}(\text{VO}_4)(\text{OH})$

Single crystal neutron diffraction data was collected at two different temperatures, 15 K and 4 K, above and below  $T_N$ . The determination of magnetic structure was done by modeling the intensities of magnetic Bragg peaks measured below the ordering temperature. A survey of the reciprocal lattice at 4 K revealed a magnetic order with the propagation vector  $\mathbf{k} = (0, 0, 0)$ . Thus, the magnetic unit cell is of the same size as the chemical cell, and the intensities measured at 4 K contain both nuclear and magnetic scattering contributions. A systematic search for magnetic models was carried out using the subtracted intensities 4 K – 15 K, that allowed separation of the magnetic and nuclear scattering, on a set of 34 unique reflections. Ultimately, refinements were carried out using combined structural and magnetic model using the 4 K data. The extinction coefficients and thermal parameters were fixed to the values obtained from the paramagnetic state, measured at 15 K. The refined structural parameters at both 15 K and 4 K are similar to those obtained from the x-ray data, listed in Table I. To understand further of the magnetic ordering temperature, order parameters were determined by following the temperature dependence of (001)

Bragg peak. Figure 6 displays the order parameter curves and it follows the power-law indicating onset of magnetic long-range ordering at 9.4 K which is a good agreement with our magnetic susceptibility and heat capacity data. The power-law equation used for fitting the order parameter data is  $I \propto m(T)^2 \propto (T_N - T)^{2\beta}$  and we found that  $\beta$  approaches to 0.25 for  $\Delta T \rightarrow 0$ , which is closed to the expected value for 2D-XY model ( $\beta \sim 0.23$ ) expected for layered magnetic structures.<sup>41</sup>

Representational theory and magnetic symmetry analysis have been employed to determine of the symmetry-allowed magnetic structure models, derived from the crystal  $P2_12_12_1$  symmetry and the wave vector  $\mathbf{k} = (0,0,0)$ . Calculations were carried out using the program SARAh Representational Analysis<sup>42</sup> and the MAXMAGN program available at the Bilbao Crystallographic Server.<sup>43</sup> The possible maximal magnetic space groups for the parent space group  $P2_12_12_1$  and the propagation vector  $\mathbf{k} = (0, 0, 0)$  are summarized in Table 3. The best fit to the data is obtained using the magnetic space group  $P2_12_12_1$ , which enable ferromagnetic spin orientation inside the chain and antiferromagnetic alignment between chains. The Wyckoff positions and the associated magnetic moments are: Co1: (0.254, 0.243, 0.495 |  $m_a, m_b, m_c$ ), Co2: (0.245, 0.757, 0.995 |  $-m_a, -m_b, m_c$ ), Co3: (0.745, 0.743, 0.005 |  $-m_a, m_b, -m_c$ ), Co4: (0.755, 0.257, 0.505 |  $m_a, -m_b, -m_c$ ). This spin configuration is different from that found in the case of Mn compound, where the magnetic order was described by the monoclinic  $P2_1$  magnetic space group that allowed the existence of an uncompensated ferromagnetic component along the  $a$ - axis. The canted structure was thought to be due to antisymmetric Dzyaloshinskii-Moriya (DM), interactions which arises from the broken inversion symmetry in SrMn(VO<sub>4</sub>)(OH). Interestingly, no symmetry lowering is required for the magnetic ordering in SrCo(VO<sub>4</sub>)(OH). In the latter, the magnetic moments are canted ( $45 \pm 3$  degrees) and follow rigidly the staggered rotation of CoO<sub>6</sub> octahedra, likely due to

spin-orbit coupling. The spins are oriented along the shortest basal bond, Co–O(1) but the canting follows opposite directions along adjacent chains. The refined moment projections are  $m_a = 2.1(1) \mu_B$ ,  $m_b = 2.1(1) \mu_B$  and  $m_c = 0.6(1) \mu_B$ . The total Co ordered moment is  $3.0(2) \mu_B$ , which is consistent with that expected for  $S = 3/2$ . The proposed magnetic structure model is depicted in Figure 7, in the form of two distinct projections along the  $c$ -axis and  $a$ -axis directions. We note that a comparable canted spin arrangement was reported for NaCoSO<sub>4</sub>F.<sup>39</sup> The spin orientation was associated with the strong magnetocrystalline anisotropy of the Co<sup>2+</sup> ion, which results from the relatively strong spin-orbit coupling.

Based on the magnetization results one can reason that an applied magnetic field along the chain direction ( $a$ -axis) could overcome the interchain antiferromagnetic coupling to flip the canting direction towards the applied field. As such, the field-induced order in SrCo(VO<sub>4</sub>)(OH) would be defined by another maximal magnetic space  $P2_1'2_1'2$ , described as the forth spin configuration in Table 3.

**Table 3.** Maximal magnetic space groups and associated Wyckoff positions and magnetic moments for the parent space group  $P2_12_12_1$  and the propagation vector  $\mathbf{k} = (0, 0, 0)$ . The four equivalent Co positions are defined as 1: (0.254, 0.243, 0.495), 2: (0.245, 0.757, 0.995), 3: (0.745, 0.743, 0.005) 4: (0.755, 0.257, 0.505).

<i>Magn. SG</i>	<u>Transformation matrix</u>	Wyckoff positions and Magnetic Moments
$P2_12_12_1$ (#19.25)	$\begin{pmatrix} 1 & 0 & 0 & 0 \\ 0 & 1 & 0 & 0 \\ 0 & 0 & 1 & 0 \end{pmatrix}$	$x, y, z \mid m_a, m_b, m_c$ ; $(-x+1/2, -y, z+1/2 \mid -m_a, -m_b, m_c)$ $(-x, y+1/2, -z+1/2 \mid -m_a, m_b, -m_c)$ $(x+1/2, -y+1/2, -z \mid m_a, -m_b, -m_c)$
$P2_1'2_1'2_1$ (#19.27)	$\begin{pmatrix} 1 & 0 & 0 & 0 \\ 0 & 1 & 0 & 0 \\ 0 & 0 & 1 & 0 \end{pmatrix}$	$(x, y, z \mid m_a, m_b, m_c)$ $(-x+1/2, -y, z+1/2 \mid -m_a, -m_b, m_c)$ $(-x, y+1/2, -z+1/2 \mid m_a, -m_b, m_c)$ $(x+1/2, -y+1/2, -z \mid -m_a, m_b, m_c)$
$P2_1'2_1'2_1$ (#19.27)	$\begin{pmatrix} 1 & 0 & 0 & 1/4 \\ 0 & 0 & -1 & 1/4 \\ 0 & 1 & 0 & 1/4 \end{pmatrix}$	$(x, y, z \mid m_a, m_b, m_c)$ $(-x+1/2, -y, z+1/2 \mid m_a, m_b, -m_c)$ $(-x, y+1/2, -z+1/2 \mid -m_a, m_b, -m_c)$ $(x+1/2, -y+1/2, -z \mid -m_x, m_b, m_c)$
$P2_1'2_1'2_1$ (#19.27)	$\begin{pmatrix} 0 & 0 & 1 & 1/4 \\ 0 & 1 & 0 & 1/4 \\ -1 & 0 & 0 & 1/4 \end{pmatrix}$	$(x, y, z \mid m_a, m_b, m_c)$ $(-x+1/2, -y, z+1/2 \mid m_a, m_b, -m_c)$ $(-x, y+1/2, -z+1/2 \mid m_a, -m_b, m_c)$ $(x+1/2, -y+1/2, -z \mid m_a, -m_b, -m_c)$

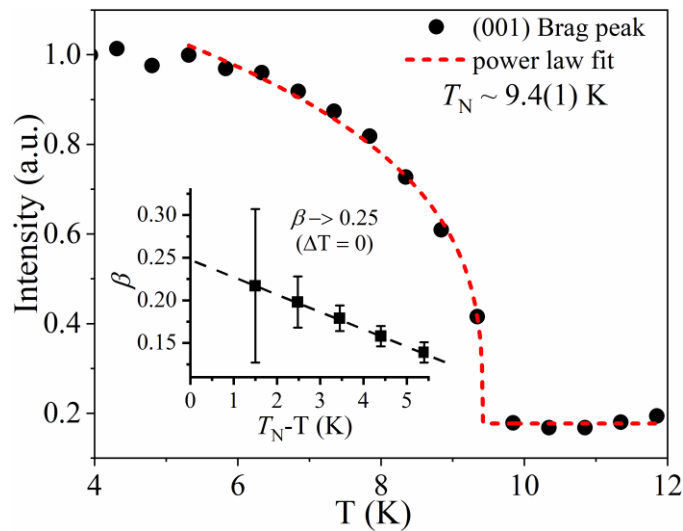


**Figure 6.** Temperature dependence of the (001) Bragg peak intensity and the fit using the power-law model as described in the text. The inset shows the critical exponent  $\beta$  associated with the magnetic order parameter as a function of fitting range ( $\Delta T$ ).

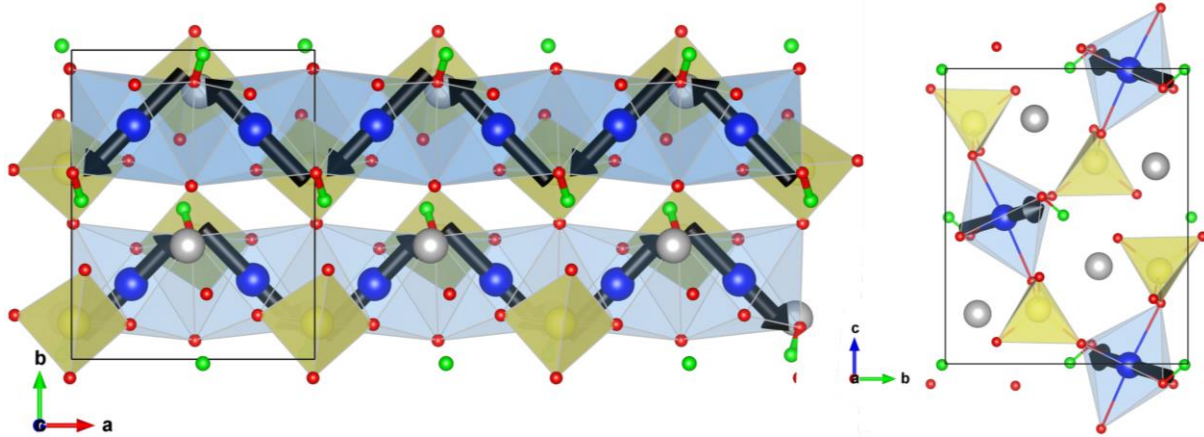


Figure 7. Magnetic structure of  $\text{SrCo}(\text{VO}_4)(\text{OH})$  at 4 K and zero field. Left panel shows the view along the  $c$ -axis, while the right panel presents a view along the  $a$ -axis (chain direction). The magnetic spins are arranged in a staggered configuration with ferromagnetic alignment along the chain and antiferromagnetic between chain, producing a fully compensated AFM ordered state.

### 3.4 Magnetic Transitions in $\text{SrCo}(\text{VO}_4)(\text{OH})$

We now discuss the phenomenological theory of the magnetization observed in  $\text{SrCo}(\text{VO}_4)(\text{OH})$ .

The system  $\text{SrCo}(\text{VO}_4)\text{OH}$  consists of  $S = 3/2$  Co(II) chains that exhibit strong magnetocrystalline anisotropy along the orbitals at approximately  $45^\circ$  from each chain. The zero-field ground state is shown in Figure 8a where neighboring chains are coupled antiferromagnetically by  $J_2 < 0$ . Spins along each  $a$ -axis chain are coupled ferromagnetically by  $J_1 > 0$ . Strong orbital anisotropy is taken along the  $\mathbf{n}_1 = (1,1,0)/\sqrt{2}$  and  $\mathbf{n}_2 = (1,-1,0)/\sqrt{2}$  directions with single-ion anisotropy constant  $K$ . Moreover, experimentally, the anisotropy  $K$  is much larger than the exchange  $J_1$  since the spins are close to the orbital directions. This could be due to strong spin-orbit coupling. As allowed by the broken inversion symmetry around each Co–Co bond in the chain, we include alternating Dzyaloshinskii-Moriya (DM) interactions between neighboring spins in the chain with constant  $D$ .

With four spins in the unit cell, the energy  $E$  per unit cell is given by

$$\begin{aligned}
E/N = & -2J_1 \{ \mathbf{S}_1 \cdot \mathbf{S}_2 + \mathbf{S}_3 \cdot \mathbf{S}_4 \} \\
& -4J_2 \{ \mathbf{S}_1 \cdot \mathbf{S}_3 + \mathbf{S}_2 \cdot \mathbf{S}_4 \} \\
& -K \{ (\mathbf{S}_1 \cdot \mathbf{n}_1)^2 + (\mathbf{S}_2 \cdot \mathbf{n}_2)^2 + (\mathbf{S}_3 \cdot \mathbf{n}_1)^2 + (\mathbf{S}_4 \cdot \mathbf{n}_2)^2 \} \\
& +2D_C \cdot \{ (\mathbf{S}_1 \times \mathbf{S}_2) + (\mathbf{S}_3 \times \mathbf{S}_4) \} \\
& -2\mu_B H \mathbf{m} \cdot \{ \mathbf{S}_1 + \mathbf{S}_2 + \mathbf{S}_3 + \mathbf{S}_4 \},
\end{aligned}$$

where  $N$  is the number of unit cells. The factor of 4 in front of  $J_2$  reflects the four neighboring chains. A magnetic field  $H$  is taken to lie along direction  $\mathbf{m}$ . For simplicity, we ignore the small components of the spins along  $c$ .

If the anisotropy  $K$  is much larger than the exchange and DM interactions, then the spins can be considered to lie along the  $\mathbf{n}_1$  or  $\mathbf{n}_2$  directions. Hence, the zero-field ground-state energy per unit cell is given by

$$E_i/N = 8J_2S^2 - 4DS^2 - 4KS^2.$$

Now consider the energies of SrCo(VO<sub>4</sub>)(OH) in magnetic fields along  $a$  or  $b$ -axes. Above the critical fields  $H_{ca}$  and  $H_{cb}$ , the spin configurations are pictured in Figure 8b and c with energies

$$\begin{aligned}
E_{ii}/N &= -8J_2S^2 - 4DS^2 - 4KS^2 - 4\sqrt{2}\mu_B HS, \\
E_{iii}/N &= -8J_2S^2 + 4DS^2 - 4KS^2 - 4\sqrt{2}\mu_B HS.
\end{aligned}$$

In all cases, the nearest-neighbor exchange energy proportional to  $J_1$  vanishes because neighboring spins are perpendicular.

Setting  $E_{ii} = E_i$  or  $E_{iii} = E_i$ , the critical fields are

$$\begin{aligned}
H_{ca} &= 2\sqrt{2}|J_2|S/\mu_B, \\
H_{cb} &= 2\sqrt{2}|J_2|S/\mu_B + \sqrt{2}DS/\mu_B \\
&= H_{ca} + \sqrt{2}DS/\mu_B.
\end{aligned}$$

Using the experimental result  $H_{ca} = 2.7$  T, we estimate that  $|J_2| \approx 0.037$  meV. Since  $H_{cb} > 7$  T, we conclude that  $D > 0.12$  meV. The magnetization induced by the field along  $a$  or  $b$  below these critical fields reflects the fact that  $K$  is not infinite. So this magnetization is proportional to small contributions of order  $|J_2|/K$ ,  $J_1/K$  and  $D/K$ . The components of the spin along  $c$ -axis may also contribute below the critical fields.

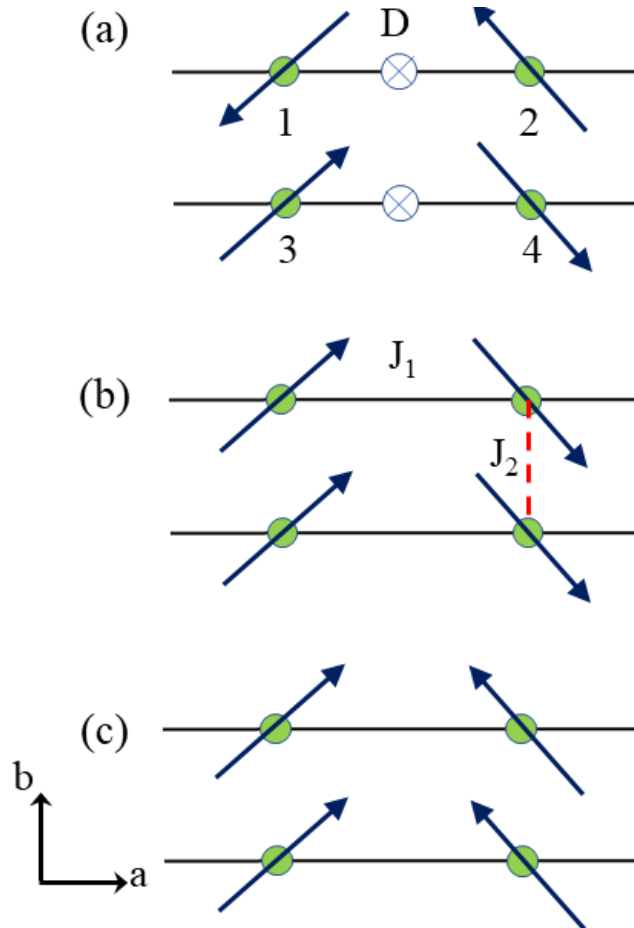


Figure 8. Three magnetic phases of  $\text{SrCo}(\text{VO}_4)(\text{OH})$ . Phase *i* (a) is stable at zero field and phases *ii* (b) and *iii* (c) are stable above critical field  $H_{ca}$  and  $H_{cb}$  for fields along the  $a$  and  $b$  directions, respectively.

#### 4. Conclusions

Single crystals of  $\text{SrCo}(\text{VO}_4)(\text{OH})$  was synthesized using the high temperature high pressure hydrothermal method. The structure of  $\text{SrCo}(\text{VO}_4)(\text{OH})$  is another addition to the adelite-descloizite mineral family which contain  $\text{Co}^{2+}$   $S = 3/2$  quasi one-dimensional magnetic chain. These chains are connected with each other via nonmagnetic tetrahedral vanadate groups. Single crystal structure was determined using X-ray single crystals diffraction technique and confirms that  $\text{SrCo}(\text{VO}_4)(\text{OH})$  crystallizes in noncentrosymmetric  $P2_12_12_1$  space group. The high temperature high pressure hydrothermal method allowed us to grow larger single crystals that can be used to determine magnetic structure using single crystal X-ray diffraction. The macroscopic magnetic measurements indicate a long-range magnetic ordering below  $T_N = 10$  K with strong anisotropy along the  $a$ -axis which is the  $\text{Co}^{2+}$  chain axis. The isothermal magnetization data along the  $a$ -axis directions exhibit a metamagnetic type transition at about 27 kOe. We noted that, magnetic properties of  $\text{SrCo}(\text{VO}_4)(\text{OH})$  are different from the iso-structural  $\text{SrMn}(\text{VO}_4)(\text{OH})$  compound. This could be due to the stronger spin-orbit couplings present in  $\text{Co}^{2+}$  and to the subtle structural difference associated with slightly smaller unit cell of  $\text{SrCo}(\text{VO}_4)(\text{OH})$  compare to the  $\text{SrMn}(\text{VO}_4)(\text{OH})$  which eventually can affect the inter-chain interactions. Single crystal neutron diffraction data revealed a magnetic structure that consists of ferromagnetic chain that are coupled antiferromagnetically. Inside the chains, the Co moments are canted to follow the staggered rotation of  $\text{CoO}_6$  octahedra, and maintain the orientation along the shortest basal bond  $\text{Co}-\text{O}(1)$ . Applied magnetic field along the chain direction induces a spin realignment that likely results in an order where the spin-canting direction is identical in all the chains. Additionally, a phenomenological model was introduced to describe the magnetic ground state at zero applied magnetic field and the field induced magnetic ground state. A very small but finite DM interaction

between next nearest Co within the chain along the  $a$ -axis was essential to describe the metamagnetic transition. The physical properties of this  $\text{Sr}M(\text{VO}_4)(\text{OH})$  ( $M = \text{Mn}$  and  $\text{Co}$ ) series suggest that a complex intra-chain and inter-chain interactions are possible and provide a fertile ground to investigate the interplay among the various magnetic ions inherited in the iso-structures. Finally, inelastic neutron scattering experiments are essential to evaluate the spin-Hamiltonian of  $\text{Sr}M(\text{VO}_4)(\text{OH})$  series in further detail.

## **ASSOCIATED CONTENT:**

### **Supporting Information**

Crystallographic refinement data from single crystal X-ray diffraction of  $\text{SrCo}(\text{VO}_4)(\text{OH})$ .

### **Accession Codes:**

CCDC 1944736 contain the supplementary crystallographic data for this paper. These data can be obtained free of charge via [www.ccdc.cam.ac.uk/data\\_request/cif](http://www.ccdc.cam.ac.uk/data_request/cif), or by emailing [data\\_request@ccdc.cam.ac.uk](mailto:data_request@ccdc.cam.ac.uk), or by contacting The Cambridge Crystallographic Data Centre, 12 Union Road, Cambridge CB2 1EZ, UK; fax: +44 1223 336033.

### **Acknowledgements:**

This work was primarily performed at Oak Ridge national laboratory Materials Sciences and Technology Division (physical property measurements) and Scientific User Facilities Division (neutron scattering) funded by US Department of Energy, Office of Science, Basic Energy Sciences. The synthesis and single crystal X-ray diffraction were performed at Clemson University and funded by the National Science Foundation under grant no. DMR-1410727.

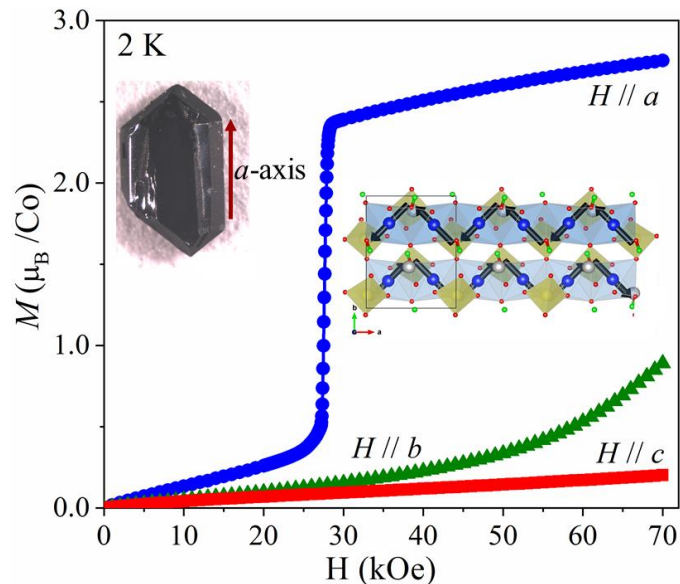
## References

- (1) Giamarchi, T. Quantum Physics in One Dimension (Oxford University Press Inc., New York, 2003).
- (2) Balents, L. Spin Liquids in Frustrated Magnets. *Nature* **2010**, *464*, 199–208.
- (3) Vasil'ev, A. N.; Markina, M. M.; Popova, E. A. Spin Gap in Lowdimensional Magnets. *Low Temp. Phys.* **2005**, *31*, 203–223.
- (4) Hase, M.; Terasaki, I.; Uchinokura, K. Observation of the Spin Peierls Transition in Linear (Spin-1/2) Chains in an Inorganic compound CuGeO<sub>3</sub>. *Phys. Rev. Lett.* **1993**, *70*, 3651–3654.
- (5) He, Z.; Kyômen, T.; Itoh, M. Quasi-one-dimensional Alternating Chain Compound with a Large Spin Gap BaCu<sub>2</sub>V<sub>2</sub>O<sub>8</sub>. *Phys. Rev. B* **2004**, *69*, 220407.
- (6) Garrett, A. W.; Nagler, S. E.; Tennant, D. A.; Sales, B. C.; Barnes, T. Magnetic Excitations in the Alternating Chain Compound (VO)<sub>2</sub>(P<sub>2</sub>O<sub>7</sub>). *Phys. Rev. Lett.* **1997**, *79*, 745–748.
- (8) Ueda, Y. Vanadate Family as Spin-Gap Systems. *Chem. Mater.* **1998**, *10*, 2653–2664
- (9) Kaul, E. E.; Rosner, H.; Yushankhai, V.; Sichelschmidt, J.; Shpanchenko, R. V.; Geibel, C.; Sr<sub>2</sub>V<sub>3</sub>O<sub>9</sub> and Ba<sub>2</sub>V<sub>3</sub>O<sub>9</sub>: Quasi-one-dimensional Spin-systems with an Anomalous Low Temperature Susceptibility. *Phys. Rev. B* **2003**, *67*, 174417.
- (10) Sanjewa, L. D.; McGuire, M. A.; Garlea, V. O.; Hu, L.; Chumanov, G.; McMillen, C. D.; Kolis, J. W. Hydrothermal Synthesis and Characterization of Novel Brackebuschite-Type Transition Metal Vanadates: Ba<sub>2</sub>M(VO<sub>4</sub>)<sub>2</sub>(OH), M = V<sup>3+</sup>, Mn<sup>3+</sup>, and Fe<sup>3+</sup>, with Interesting Jahn–Teller and Spin-Liquid Behavior. *Inorg. Chem.* **2015**, *54*, 7014–7020.
- (11) Cheng, J.; Tian, W.; Zhou, J.; Lynch, V. M.; Steinfink, H.; Manthiram, A.; May, A. F.; Garlea, V. O.; Neuefeind, J. O.; Yan, J. Crystal and Magnetic Structures and Physical Properties of a New Pyroxene NaMnGe<sub>2</sub>O<sub>6</sub> Synthesized Under High Pressure. *J. Am. Chem. Soc.* **2013**, *135*, 2776–2786.
- (12) He, Z.; Taniyama, T.; Kyômen, T.; Itoh, M. Field-induced Order-disorder Transition in the Quasi-one-dimensional Anisotropic Antiferromagnet BaCo<sub>2</sub>V<sub>2</sub>O<sub>8</sub>. *Phys. Rev. B* **2005**, *72*, 172403.
- (13) Garlea, V. O.; Sanjewa, L. D.; McGuire, M. A.; Kumar, P.; Sulejmanovic, D.; He, J.; Hwu, S.-J. Complex Magnetic Behavior of the Sawtooth Fe Chains in Rb<sub>2</sub>Fe<sub>2</sub>O(AsO<sub>4</sub>) *Phys. Rev. B* **2014**, *89*, 014426.
- (14) McMillen, C. D.; Kolis, J. W. Hydrothermal Synthesis as a Route to Mineralogically-Inspired Structures. *Dalton Trans.* **2016**, *45*, 2772–2784.
- (15) Streltsov, S. V.; Khomskii, D. I. Electronic Structure and Magnetic Properties of Pyroxenes (Li,Na)TM(Si,Ge)<sub>2</sub>O<sub>6</sub>: Low-dimensional Magnets with 90° Bonds. *Phys. Rev. B* **2008**, *77*, 064405.
- (16) Millet, P.; Mila, F.; Zhang, F. C.; Mambrini, M.; Van Oosten, A. B.; Pashchenko, V. A.; Sulpice, A.; Stepanov, A. Biquadratic Interactions and Spin-Peierls Transition in the Spin-1 Chain LiVGe<sub>2</sub>O<sub>6</sub>. *Phys. Rev. Lett.* **1999**, *83*, 4176.
- (17) Zhang, S.; Xiang, H.; Guo, W.; Tang, Y.; Cuia, M.; He, Z. Synthesis, Characterization, and Mechanism Analysis of S = 2 Quasi-One-Dimensional Ferromagnetic Semiconductor Pb<sub>2</sub>Mn(VO<sub>4</sub>)<sub>2</sub>(OH). *Dalton Trans.* **2016**, *45*, 7022–7027.
- (18) Effenberger, H.; Krause, W.; Bernhardt, H. J. Ninth International Symposium on Experimental Mineralogy, Petrology and Geochemistry, Vol. 9 (Zurich, Switzerland, 2002), p. 30.

- (19) Hawthorne, F. C.; Faggiani, R. Refinement of the Structure of Deseloizite. *Acta Cryst. B* **1979**, *35*, 717.
- (20) Sanjeeva, L. D.; Garlea, O. V.; McGuire, M. A.; McMillen, C. D.; Cao, H.; Kolis, J. W. Structural and Magnetic Characterization of the One-Dimensional  $S = 5/2$  Antiferromagnetic Chain System  $\text{SrMn}(\text{VO}_4)(\text{OH})$ . *Phys. Rev. B* **2016**, *93*, 224407.
- (21) Garlea, V. O.; Sanjeeva, L. D.; McGuire, M. A.; Batista, C. D.; Samarakoon, A. M.; Graf, D.; Winn, B.; Ye, F.; Hoffmann, C.; Kolis, J. W. Exotic Magnetic Field-Induced Spin-Superstructures in a Mixed Honeycomb-Triangular Lattice System *Phys. Rev. X* **2019**, *9*, 011038.
- (22) Sanjeeva, L. D.; McMillen, C. D.; Willett, D.; Chumanov, G.; Kolis, J. W. Hydrothermal Synthesis of Single Crystals of Transition Metal Vanadates in the Glaserite Phase. *J. Solid State Chem.* **2016**, *236*, 61–68.
- (23) Sanjeeva, L. D.; McMillen, C. D.; McGuire, M. A.; Kolis, J. W. Manganese Vanadate Chemistry in Hydrothermal  $\text{BaF}_2$  Brines:  $\text{Ba}_3\text{Mn}_2(\text{V}_2\text{O}_7)\text{F}_2$  and  $\text{Ba}_7\text{Mn}_8\text{O}_2(\text{VO}_4)_2\text{F}_{23}$ . *Inorg. Chem.* **2016**, *55*, 12512–12515.
- (24) Sanjeeva, L. D.; McGuire, M. A.; McMillen, C. D.; Willett, D.; Chumanov, G.; Kolis, J. W. Honeycomb-like  $S = 5/2$  Spin Lattices in New Manganese(II) Vanadates. *Inorg. Chem.* **2016**, *55*, 9240–9249.
- (25) Taddei, K. M.; Sanjeeva, L. D.; Kolis, J. W.; Sefat, A. S.; Cruz, C.; Pajerowski, D. M. Local-Ising-Type Magnetic Order and Metamagnetism in the Rare-Earth Pyrogermanate  $\text{Er}_2\text{Ge}_2\text{O}_7$ . *Phys. Rev. Mater.* **2019**, *3*, 014405.
- (26) Natarajan, S.; Mandal, S. Open-Framework Structures of Transition-Metal Compounds. *Angew. Chem. Int. Ed.* **2008**, *47*, 4798–4828.
- (27) Hwu, S.-J. Structurally Confined Transition-Metal Oxide Layers, Chains and Oligomers in Molecular and Extended Magnetic Solids. *Chem. Mater.* **1998**, *10*, 2846–2859.
- (28) Krivovichev S. V.; Which Inorganic Structures are the Most Complex? *Angew. Chem. Int. Ed.* **2014**, *53*, 654–661.
- (29) Geertsma W.; Khomskii, D. Influence of Side Groups on  $90^\circ$  Superexchange: A Modification of the Goodenough-Kanamori-Anderson Rules. *Phys. Rev. B* **1996**, *54*, 3011.
- (30) CrystalClear; Rigaku and Molecular Structure Corporation: The Woodlands, TX, 2006.
- (31) Sheldrick, G. M. A Short History of SHELX. *Acta Crystallogr. A* **2008**, *64*, 112–122.
- (32) Chakoumakos, B. C.; Cao, H. B.; Ye, F.; Stoica, A. D.; Popovici, M.; Sundaram, M.; Zhou, W.; Hicks, J. S.; Lynn, G. W.; Riedel, R. A.; Four-circle Single-crystal Neutron Diffractometer at the High Flux Isotope Reactor.", *J. Appl. Cryst.* **2011**, *44*, 655–658.
- (33) He, Z.; Yamaura, J.-I.; Ueda, Y.; Cheng, W.  $\text{CoV}_2\text{O}_6$  Single Crystals Grown in a Closed Crucible: Unusual Magnetic Behaviors with Large Anisotropy and  $1/3$  Magnetization Plateau. *J. Am. Chem. Soc.* **2009**, *131*, 7554–7555.
- (34) He, Z.; Taniyama, T.; Itoha, M.; Large Magnetic Anisotropy in the Quasi-one-dimensional System  $\text{BaCo}_2\text{V}_2\text{O}_8$ . *Appl. Phys. Lett.* **2006**, *88*, 132504.
- (35) Rodriguez, E. E.; Cao, H.; Haiges, R.; Melot, B. C. Single Crystal Magnetic Structure and Susceptibility of  $\text{CoSe}_2\text{O}_5$ . *J. Solid State Chemistry* **2016**, *236*, 39–44.
- (36) Melot, B. C.; Paden, B.; Seshadri, R. Magnetic Structure and Susceptibility of  $\text{CoSe}_2\text{O}_5$ : An Antiferromagnetic Chain Compound. *Phys. Rev. B* **2010**, *82*, 014411.
- (37) He, Z.; Guo, W.; Cui, M.; Tang, Y. Synthesis and Magnetic Properties of New Tellurate Compounds  $\text{Na}_4\text{MTeO}_6$  ( $M = \text{Co}$  and  $\text{Ni}$ ) with a Ferromagnetic Spin-chain Structure. *Dalton Trans.*, **2017**, *46*, 5076–5081

- (38) Bera, A. K.; Lake, B.; Stein, W. D.; Zande, S.; Magnetic Correlations of the Quasi-one-dimensional Half-integer Spin-chain Antiferromagnets  $\text{SrM}_2\text{V}_2\text{O}_8$  ( $M = \text{Co}, \text{Mn}$ ). *Phys. Rev. B* **2014**, *89*, 094402.
- (39) Melot, B. C.; Rousse, G.; Chotard, J.-N.; Kemei, M. C.; Rodriguez-Carvajal, J.; Tarascon, J.-M. Magnetic Structure and Properties of  $\text{NaFeSO}_4\text{F}$  and  $\text{NaCoSO}_4\text{F}$ . *Phys. Rev. B* **2012**, *85*, 094415.
- (40) Zhang, S.-Y.; Guo, W.-B. Tang, Y.-Y.; Xu, J.-Q.; He, Z.-Z. Observation of Spin Relaxation in a Vanadate Chloride with Quasi One-Dimensional Linear Chain. *Cryst. Growth Des.* **2019**, *19*, 2228–2234.
- (41) Bramwell, S. T.; Holdsworth, P. C. W. Magnetization and Universal Sub-critical Behaviour in Two-dimensional XY Magnets. *J. Condens. Matter Phys.* **1993**, *5*, L53.
- (42) Wills, A. S. A New Protocol for the Determination of Magnetic Structures Using Simulated Annealing and Representational Analysis (SARAh). *Physica B:Condensed Matter* **2000**, *276*, 276–278.
- (43) Perez-Mato, J. M.; Gallego, S. V.; Tasci, E. S.; Elcoro, L.; Flor, G.; Aroyo, M. I.; Symmetry-Based Computational Tools for Magnetic Crystallography. *Annu. Rev. Mater. Res.* **2015**, *45*, 217–248.

For Table of Contents Use Only:



Single crystals of  $\text{SrCo}(\text{VO}_4)(\text{OH})$  were synthesized using high-temperature high-pressure hydrothermal method. The magnetic measurements exhibit a large magnetic anisotropy with a field induced magnetic transition when the applied magnetic field along the  $a$ -axis (Co–O–Co chain axis). The magnetic spins are canted along the  $a$ -axis giving a net ferromagnetism along the chain direction and couple antiferromagnetically between chains.